Available online at www.sciencedirect.com

ScienceDirect

Procedia CIRP 131 (2025) 107–112

www.elsevier.com/locate/procedia

3rd CIRP Conference on Composite Material Parts Manufacturing

Temperature distribution inside composite and fiber metal laminates during modified cure cycles

Johannes Wiedemann*[a], Tetiana Pittsyk[a], Oliver Völkerink[a], Christian Hühne[a,b]

[a]*TU Braunschweig, Institute of Mechanics and Adaptronics, Langer Kamp 6, 38106 Braunschweig, Germany*
[b]*DLR, German Aerospace Center, Institute of Lightweight Systems, Lilienthalplatz 7, 38108 Braunschweig, Germany*

* Corresponding author. Tel.: +49-531-391-8077 ; *E-mail address:* johannes.wiedemann@tu-braunschweig.de

Abstract

Manufacturing-induced thermal residual stresses reduce the mechanical strength of fiber metal laminates (FML). Modified (MOD) cure cycles can help to reduce these stresses. However, the typically assumed homogeneous temperature distribution across the thickness of a laminate may not hold true for laminate configurations with, e.g., large thicknesses or low thermal conductivity. Therefore, the temperature in monolithic composite and fiber metal laminates is experimentally determined. Based on the experimental results, a numerical heat transfer model is developed to predict the temperature throughout the cure cycle. A good agreement between experiment and simulation is achieved. The numerical model further shows that temperature gradients of up to 20 °C for a 40 mm thick laminate can be expected, which will significantly influence the homogeneity of the residual stress state in such a laminate manufactured with a MOD cycle. The numerical model can serve as a valuable tool for estimating the homogeneity of the temperature distribution across the thickness of a laminate for different layups and cure cycle modifications.

Keywords: fiber metal laminates; thermal residual stress; cure cycle modification; heat transfer; composite manufacturing

1. Introduction

Fiber metal laminates (FML) consist of alternating layers of thin metal sheets and fiber-reinforced polymer (FRP) plies. Based on the metal volume fraction (MVF) used, the resulting laminate maintains relatively high specific stiffness and strength compared to FRP materials. However, due to the metal's ductility, it exhibits significantly better impact and fatigue resistance as well as load-bearing capability than monolithic composites. These characteristics make FMLs suitable for a wide variety of applications. [1, 2]

However, due to the different coefficients of thermal expansion between FRP and metal, the stiffnesses of the single layers in the laminate, and the elevated temperature during manufacturing, thermally-induced residual stresses evolve during cure. The residual stress state generally consists of tensile stresses in the metal layers and compressive stresses in the fiber layers in the fiber direction [3, 4]. These stresses significantly reduce the mechanical material strength both for quasi-static [5] and dynamic loading [6] and the influence even increases for lower operating temperatures, i.e., larger temperature differences compared to the bonding temperature during manufacturing [7].

Therefore, different methods have been investigated in the past on how to reduce these manufacturing-induced residual stresses. These methods include post-stretching [8], clamping fixtures during manufacturing [9] and cure cycle modifications [10, 11]. The latter has proven to be the most versatile approach and is also applicable for complex part geometries and orthotropic layups.

The applicability of modified cure cycles, sometimes called smart cure cycles, has been shown mainly on a coupon level. Past publications investigated the influence of these cycle variations on mechanical or asymmetric test specimens. However, due to the importance of the temperature profile in these cure cycles, it is questionable whether these modifications can also be applied to large-scale FML structures. When applying modified cure cycles to reduce residual stresses in an FML, a homogeneous temperature distribution inside the laminate throughout the cure cycle is necessary to achieve a homogeneous stress state in the laminate. Prussak et al. [12] showed that a temperature difference of 5 °C when cooling is initiated or a difference

10.1016/j.procir.2024.10.333

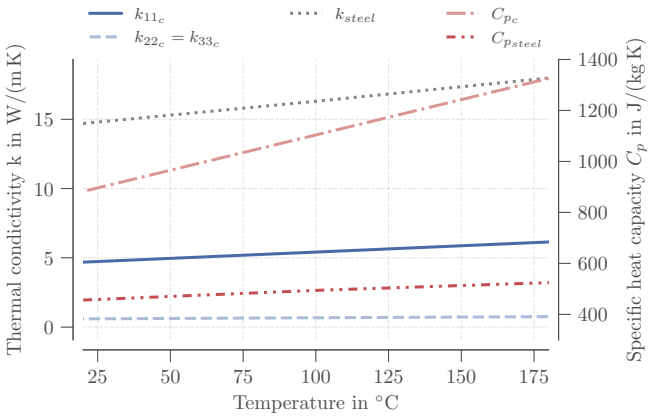

Fig. 1. Thermal conductivity and specific heat capacity dependent on temperature for the composite (c) and steel materials used in this work.

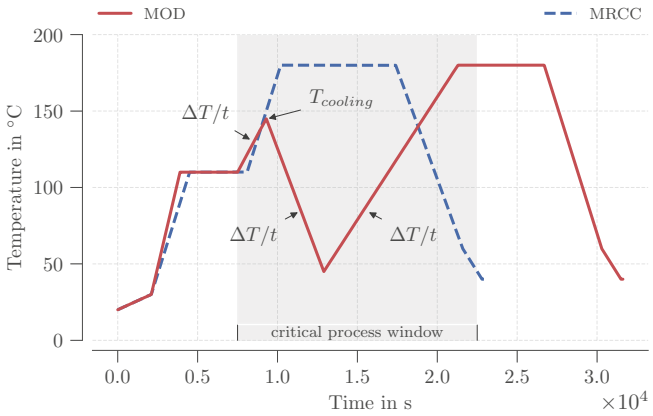

Fig. 2. Temperature profiles of the modified (MOD) and the manufacturer-recommended cure cycle (MRCC). The shaded area illustrates the stage in the MOD cycle where the residual stress state of a laminate is mainly determined, and process control is critical.

in the heating or cooling ramps of 2 °C/min can make a significant difference in the resin cure kinetics.

The laminate's heat capacity and thermal conductivity govern the temperature distribution throughout the cure cycle. It is assumed that with increasing laminate thickness and component size, the higher heat capacity combined with the low thermal conductivity of the polymer layers will increase the temperature difference between the inside and outside of a laminate. Eventually, this can lead to an inhomogeneous stress state in a laminate, reducing the effect of the modified cure cycles.

Therefore, this study aims to investigate the uniformity of the temperature distribution across the thickness during manufacturing using modified curing cycles. Based on experimental data, a numerical model is developed. It is assumed that low metal volume fractions and thicker cross-sections lead to slower heat transfer into and out of a laminate due to the lower thermal conductivity and higher heat capacity of the polymer compared to metal. Therefore, monolithic FRP laminates without additional metal layers are the focus of the investigations, providing results that can be assumed to serve as an upper limit of expected temperature differences.

2. Materials and methods

2.1. Materials

The laminates in this work are manufactured using a carbon fiber-reinforced epoxy prepreg (Hexcel Hexply 8552-AS4) and a stainless steel alloy (X10CrNi18-8, DIN 1.4310, AISI 301). For the numerical model, the thermal conductivity k_c and specific heat capacity C_{p_c} for the CFRP material are taken from [13]. Fig. 1 shows the composite thermal properties in the fiber direction (11) and transverse to the fiber direction (22) in dependence of the temperature for a degree of cure of 100 %. A detailed formulation of the thermal properties is provided in the Appendix A.

For the FML steel sheets the thermal conductivity k_{steel} and specific heat capacity $C_{p_{steel}}$ are also plotted in Fig. 1 based on [14]. Since the manufacturing tool is also made of stainless steel, the same material properties are assumed for the tool.

2.2. Cure cycle

The modified cure cycle developed for the Hexcel 8552 matrix material and used in this work is based on [12]. The cure cycle was already extensively used in previous works [4, 15]. The MOD cycle has been shown to decrease the residual stresses in FML laminates made of CFRP and steel by around 27 % [16], which can significantly increase the quasi-static and fatigue performance of different FML layups [6]. The temperature profile of the MOD cure cycle is illustrated in Fig. 2, with the manufacturer-recommended cure cycle (MRCC) given as a reference. The critical process window in which the temperature control in the cure cycle must be very precise is shaded in the figure. The heating and cooling rates ($\Delta T/t$) and the temperature at which cooling is initiated ($T_{cooling}$) are of particular importance. During this stage in the process, the resin changes its mechanical behavior from viscous to visco-elastic at gelation and eventually to elastic at vitrification. From gelation onwards, the resin is able to transfer loads, which is a requirement for the residual stress evolution. The final residual stress state at room temperature depends on the temperature at which the initially independent layers of the laminate start to bond, which happens after the transition of the resin into the visco-elastic state.

2.3. Experimental setup

Different laminates are manufactured with the MOD cycle to get an understanding of temperature distribution during manufacturing. These are an FML laminate ($[(St/0°_4)_5/\overline{St}]_S$) with a total laminate thickness of 6.52 mm and a metal volume fraction (MVF) of 20.2 % and a monolithic cross-ply CFRP laminate with a laminate thickness of 20 mm. Due to the combination of these measurements with other investigations, the two laminates have different in-plane geometries (FML: 200 mm ×

Table 1. Position of thermocouples in the investigated laminates, in respect to the laminate thickness coordinate z which ranges from 0 % (bottom = tool side) to 100 % (top = vacuum bag side).

	TC1	TC2	TC3	TC4
FML	6 %	35 %	65 %	94 %
CFRP	3 %	26 %	50 %	82 %

200 mm, CFRP: 125 mm × 125 mm). However, the small in-plane geometrical differences of the laminates are assumed to not influence the through-thickness temperature distribution.

For the temperature measurements, thermocouples (TCs) of type K are placed in the center of the laminates during the layup. Table 1 gives the positions with respect to the laminate thickness for the FML and CFRP laminate. The positions in the laminates were defined based on previous assumptions and the same TC positions are used in the numerical simulation.

The laminates are manufactured using a standard prepreg lamination process on a steel tool under full vacuum and additional pressure of 0.7 MPa during cure in an autoclave. Further details on the manufacturing process can be found, e.g., in [4].

2.4. Numerical model

The numerical simulations of the temperature distribution are performed using Abaqus heat transfer analysis. A 3D model of the laminates, including the steel tool, is created and meshed with 20-node quadratic brick elements (DC3D20) to extend the model for more complex part geometries in the future, and since computational efficiency is not a concern. All the elements in the model are given a temperature of 293 K in the initial step in the form of a predefined field.

For the transient step, several simplifications are made. The thermal material parameters (thermal conductivity and specific heat capacity) are only assumed to be temperature-dependent. Although the dependence on the degree of cure is reported in several works, e.g., [17], it is neglected to reduce the modeling effort. From the formulas derived by [13] and provided in the Appendix A, it can be found that the influence of the degree of cure is significantly smaller than the temperature influence, and therefore, this simplification in the model seems acceptable. Furthermore, the temperature in the transient step is applied as a surface film condition with the autoclave temperature defined through an amplitude over the duration of the cure cycle.

Slesinger et al. [18] show that the heat transfer coefficient (HTC) for the circulating hot air depends on the location inside the autoclave. For the investigated setup, the HTCs varied between 60 W/(m^2 K) and 200 W/(m^2 K) depending on the airflow. A value of 100 W/(m^2 K) is observed around the area where the tool with the laminate is placed. Although the autoclave used in this work differs, the value is used in the numerical model on the top ply of the laminate and the bottom of the steel tool as the initial starting value. The other surfaces of the laminates are assumed to be adiabatic.

To further improve the numerical model based on the experimental results, the material parameters are kept constant, and only the HTCs at the top and bottom of the laminate are treated as variables. The HTCs are then adjusted to minimize the deviations of the temperatures at the individual thermocouple positions between the simulation and the experiment.

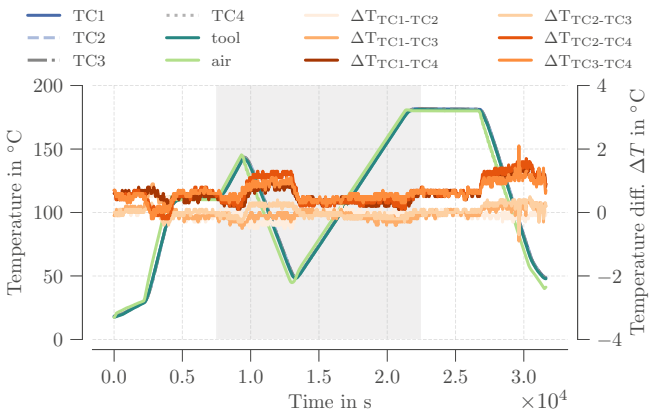

Fig. 3. Temperatures measured during manufacturing of the FML with the MOD cycle and corresponding temperature differences inside the laminate.

3. Results

3.1. Experimental temperature distribution

The measured temperatures over time throughout the MOD cycle for the FML specimen are shown in Fig. 3. Additionally, the temperatures of the tool and autoclave air are shown. The tool and TC temperatures show only minor differences, so the curves can hardly be differentiated in the figure. In contrast, the air temperatures always precede the temperatures measured inside the laminate, as the autoclave regulates the air temperature, which then circulates around the tool and the vacuum bag enclosing the laminate. The maximum deviation between all the thermocouples inside the FML is below 2 °C during the final cool-down step in the cure cycle. However, the residual stress state is already determined at this stage in the cure cycle. When looking at the relevant stage of the cure cycle (shaded area), the highest deviation is found to be 1.3 °C during the intermediate cooling step.

Compared to the 5 °C difference discussed in [12], the difference is assumed to be too small to result in significant deviations of the residual stress state across the laminate. Therefore, the development of a homogeneous residual stress state in such an FML with a thickness of 6.52 mm and an MVF of 20.2 % can be assumed.

The temperatures for the 20 mm thick CFRP specimen are plotted in Fig. 4. Here, the difference between the air and tool temperature and the temperatures inside the laminate is more pronounced due to the laminate's higher heat capacity and lower thermal conductivity. In this case, also significantly higher deviations between the different thermocouples can be found. Again, the highest temperature difference is found in the last curing stage, which is irrelevant for residual stress forma-

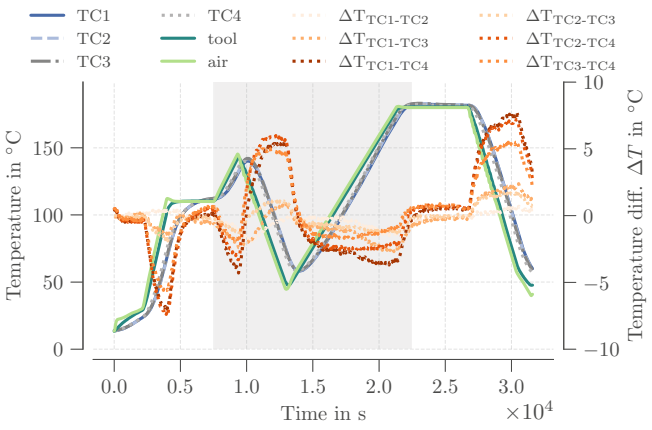

Fig. 4. Experimental temperatures and temperature differences inside the laminate during the MOD cycle for a 20 mm thick CFRP laminate.

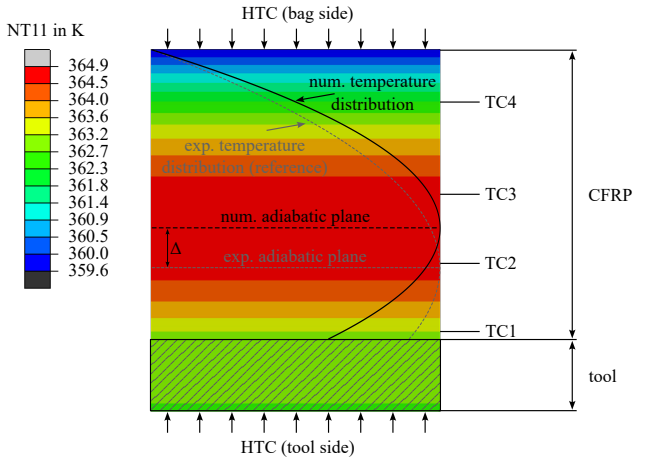

Fig. 5. Cross-sectional view of the numerical model with the nodal temperature (NT) distribution during the intermediate cooling step for the initial HTC values and experimental temperature distribution given as a reference.

tion. It can be seen that the temperature in the laminate differs by around 5 °C during intermediate cooling between the thermocouple being furthest away from the tool (TC4) and the other three thermocouples (TC1, TC2, TC3).

3.2. Numerical temperature distribution

The numerical simulation is validated using the 20 mm thick CFRP laminate. Fig. 5 shows a cross-section of the numerical model and the nodal temperature (NT) distribution across the thickness at a selected time increment during the intermediate cooling step in the MOD cycle. The figure further shows the tool, the thermocouple positions, and the adiabatic plane in the laminate. The adiabatic plane defines the position in the thickness direction across which no heat is transferred. The adiabatic plane is not in the symmetry plane of the laminate, although the layup is symmetric because, on the bottom side, the heat is transferred through the tool, and on the top side, it is directly transferred to the laminate.

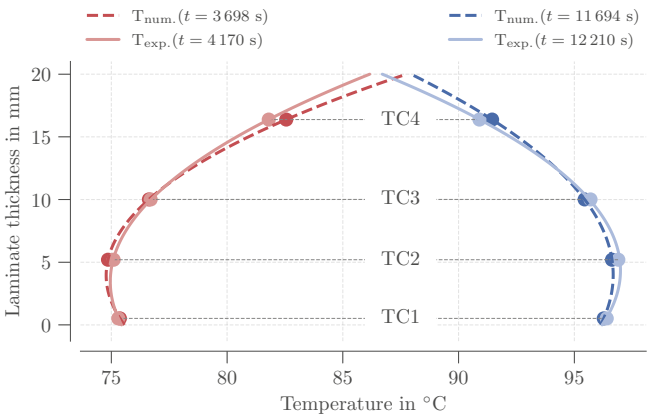

Fig. 6. Experimental and numerical (updated HTCs) temperature distribution across the thickness of the 20 mm CFRP laminate, with data points indicating the TC locations and lines representing the parabolic fit.

When comparing the experimental reference curve and the numerical temperature distribution in Fig. 5, the numerical adiabatic plane is shifted towards the center of the laminate. This leads to the conclusion that more heat is transferred through the tool side in the numerical model compared to the experiment. Hence the initially assumed values for the HTCs (100 W/(m^2 K)) from the literature do not seem to represent the experimental setup used in this work. Therefore, the HTCs are iteratively updated until the numerical temperature distribution and adiabatic plane match the experimental results.

The model updating results in HTCs of 80 W/(m^2 K) at the top of the laminate and 40 W/(m^2 K) at the bottom of the tool. With these values, the experimental temperature distribution across the thickness of the laminate is very well represented in the numerical model. This is shown in Fig. 6, where the temperatures of the four TC positions are plotted over the laminate thickness for selected time increments during the initial heating and the intermediate cooling stage in the cure cycle. Slight differences in the time increments between the experiment and the simulation originate from the different increment sizes but do not affect the comparability. The increments were chosen so that the experimental and numerical temperatures at the position TC1 are identical. Based on the results of [19], the temperature distribution across the thickness can be assumed to follow a second-order polynomial. Fitting a quadratic function through the data points by minimizing the sum of the squared residuals demonstrates an appropriate fit for both the experimental and numerical results. The vertex of the corresponding parabola defines the adiabatic plane in the laminate. A very good agreement between experimental and numerical results is achieved both during heating and cooling.

In Fig. 7, the experimental and numerical temperature differences between all TC positions are plotted over the cure cycle. Additionally, the absolute temperature of the numerical TC1 is given as a reference. The overall results show that the numerical model can very accurately represent the temperature distribution as measured during the experiment over the entire cure cycle.

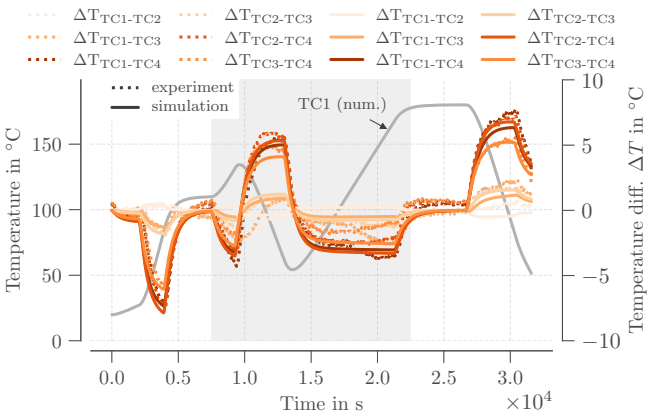

Fig. 7. Comparison of the numerical and experimental temperatures at the TC positions inside the 20 mm thick CFRP laminate during the MOD cycle.

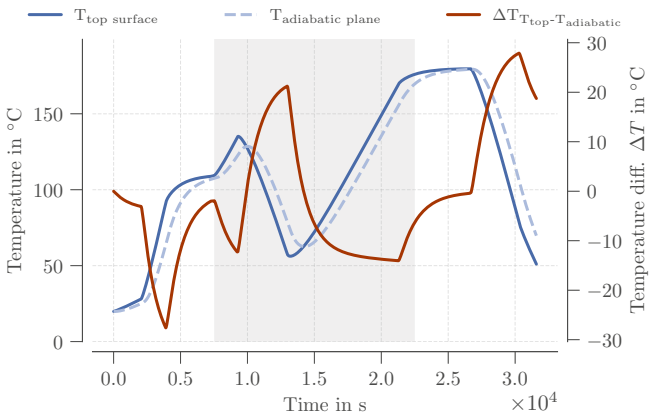

Fig. 8. Numerical temperature distribution during MOD cycle of a 40 mm thick CFRP laminate shows significant differences between the top laminate surface and the adiabatic plane in the laminate.

4. Discussion

Although the simulation makes several simplifications, the numerical model can accurately describe the temperature distribution inside a CFRP laminate during manufacturing using modified cure cycles. Therefore, the model is used to additionally simulate a 40 mm thick CFRP laminate, a laminate thickness that is common at the wing root joint of an aircraft [20]. The temperatures throughout the cure cycle are shown in Fig. 8 for the top surface and adiabatic plane of the laminate. The results indicate an expected temperature difference of up to 20 °C between the two locations in the critical process window. Furthermore, the temperature at the point in the MOD cycle when curing is initiated ($T_{cooling}$ in Fig. 2) significantly deviates between the two positions in the laminate. These deviations can lead to considerable differences in the cure kinetics of the resin [12], leading to different bonding temperatures between the plies and, hence, to substantial differences in the residual stress state. However, for these very thick composite laminates, the exothermic reaction of the resin might not be neglected anymore and can further influence the results.

The results show that a homogeneous temperature distribution during modified cure cycles can no longer be expected for unfavorable laminates with large thicknesses, low thermal conductivity, and high specific heat capacity.

5. Conclusion

Modified cure cycles are used to reduce manufacturing-induced thermal residual stresses in FML. Application of the MOD cycles generally assumes a homogeneous temperature distribution throughout the laminate. Temperature measurements in fiber metal laminates and monolithic CFRP laminates showed that the temperature gradient across the laminate thickness during critical stages of a modified cure cycle can be significant. Temperature deviations of up to 5 °C for a 20 mm thick CFRP laminate can already influence the local cure kinetics in a specimen's cross-section. A numerical model was developed based on the experimental results to predict the temperature distribution inside a laminate. After updating the heat transfer coefficients at the surfaces, the model yielded very accurate results compared to the experimental measurements. Consequently, the model can serve as a tool to estimate the temperature distribution throughout a modified cure cycle for a laminate of interest and subsequently help to optimize the cure cycle towards a smaller temperature gradient and, hence, a more homogeneous residual stress state.

Acknowledgements

The authors expressly acknowledge the financial support for the research work on this article within the Research Unit 3022, "Ultrasonic Monitoring of Fibre Metal Laminates Using Integrated Sensors" by the German Research Foundation (Deutsche Forschungsgemeinschaft (DFG)).

CRediT authorship contribution statement

Johannes Wiedemann: Conceptualization, Data Curation, Formal Analysis, Investigation, Methodology, Validation, Visualization, Writing - Original Draft, Writing - Review and Editing. **Tetiana Pittsyk:** Data Curation, Formal Analysis, Methodology, Validation, Visualization, Writing - Review and Editing. **Oliver Völkerink:** Funding acquisition, Project administration, Resources, Writing - Review and Editing. **Christian Hühne:** Funding acquisition, Project administration, Resources, Writing - Review and Editing.

Appendix A. Thermal properties of prepreg 8552-AS4

The correlations to derive composite properties from fiber and resin properties and the thermal material characterization for the 8552-AS4 prepreg are based on the work of Johnston [13] and presented in the following. The specific heat ca-

pacity of the composite C_{P_c} from fiber C_{P_f} and resin C_{P_r} properties can be derived using a simple rule of mixture and the fiber volume fraction V_f:

$$C_{P_c} = V_f C_{P_f} + (1 - V_f) C_{P_r} \tag{A.1}$$

Likewise, the thermal conductivity in the fiber direction k_{11_c} of the composite can be derived by the fiber k_{11_f} and resin k_r conductivities:

$$k_{11_c} = V_f k_{11_f} + (1 - V_f) k_r \tag{A.2}$$

For the composite thermal conductivity in the transverse k_{22_c} and thickness direction k_{33_c}, a more comprehensive equation originally proposed by [21] is needed:

$$k_{22_c} = k_{33_c} = \\ = k_r \left(\left(1 - 2\sqrt{\frac{V_f}{\pi}} \right) + \frac{1}{B} \left(\pi - \frac{4}{A} \tan^{-1} \frac{A}{1 + B\sqrt{\frac{V_f}{\pi}}} \right) \right) \tag{A.3}$$

$$\text{with} \quad A = \sqrt{1 - \frac{B^2 V_f}{\pi}}, \text{ and} \quad B = 2\left(\frac{k_r}{k_{22_f}} - 1 \right) \tag{A.4}$$

A detailed characterization of the 8552-AS4 prepreg material is provided by [13]. The specific heat capacities for the fibers C_{P_f} and for the resin C_{P_r} were derived as:

$$\begin{aligned} C_{P_f} &= 904 + 2.05\,(T - 75)\,/^\circ\text{C} \\ C_{P_r} &= 1005 + 3.74\,(T - 20)\,/^\circ\text{C} \end{aligned} \tag{A.5}$$

The thermal conductivities in fiber direction k_{11_f}, fiber transverse direction k_{22_f} and for the resin k_r are given by:

$$\begin{aligned} k_{11_f} &= 7.69 + 1.56 \times 10^{-2} T/^\circ\text{C} \\ k_{22_f} &= 2.4 + 5.07 \times 10^{-3} T/^\circ\text{C} \\ k_r &= 0.148 + 3.43 \times 10^{-4} T/^\circ\text{C} + 6.07 \times 10^{-2} \alpha \end{aligned} \tag{A.6}$$

with α being the degree of cure.

References

[1] A. Vlot, J. W. Gunnink, Fibre metal laminates: An introduction, Springer Netherlands, Dordrecht, 2001. URL: https://ebookcentral.proquest.com/lib/gbv/detail.action?docID=3565888.

[2] T. Sinmazçelik, E. Avcu, M. Ö. Bora, O. Çoban, A review: Fibre metal laminates, background, bonding types and applied test methods, Materials & Design 32 (2011) 3671–3685. doi:10.1016/j.matdes.2011.03.011.

[3] M. Abouhamzeh, Distortions and residual stresses of GLARE induced by manufacturing, Ph.D. thesis, Delft University of Technology, 2016. doi:10.4233/uuid:1f1b3e5c-72b8-440c-8d98-4b4c82814fb6.

[4] J. Wiedemann, R. Prussak, E. Kappel, C. Hühne, In-situ quantification of manufacturing-induced strains in fiber metal laminates with strain gages, Composite Structures Vol. 691 (2022) 115967. doi:10.1016/j.compstruct.2022.115967.

[5] E. Kappel, R. Prussak, J. Wiedemann, On a simultaneous use of fiber-Bragg-gratings and strain-gages to determine the stress-free temperature Tsf during GLARE manufacturing, Composite Structures 227 (2019). doi:10.1016/j.compstruct.2019.111279.

[6] J. Wiedemann, S. Mrzljak, C. Hühne, F. Walther, Increased accuracy of service life prediction for fiber metal laminates by consideration of the manufacturing-induced residual stress state: Proceedings of the 10th European Workshop on Structural Health Monitoring (EWSHM 2024), e-Journal of Nondestructive Testing 29 (2024). doi:10.58286/29832.

[7] J. Koord, O. Völkerink, E. Petersen, C. Hühne, Effect of low temperature on mode I and mode II interlaminar fracture toughness of CFRP-steel hybrid laminates, Composites Part B: Engineering 262 (2023) 110773. doi:10.1016/j.compositesb.2023.110773.

[8] S. U. Khan, R. C. Alderliesten, R. Benedictus, Post-stretching induced stress redistribution in Fibre Metal Laminates for increased fatigue crack growth resistance, Composites Science and Technology 69 (2009) 396–405. doi:10.1016/j.compscitech.2008.11.006.

[9] J. Xue, W.-X. Wang, Y. Takao, T. Matsubara, Reduction of thermal residual stress in carbon fiber aluminum laminates using a thermal expansion clamp, Composites Part A: Applied Science and Manufacturing 42 (2011) 986–992. doi:10.1016/j.compositesa.2011.04.001.

[10] H. S. Kim, S. W. Park, D. G. Lee, Smart cure cycle with cooling and reheating for co-cure bonded steel/carbon epoxy composite hybrid structures for reducing thermal residual stress, Composites Part A: Applied Science and Manufacturing 37 (2006) 1708–1721. doi:10.1016/j.compositesa.2005.09.015.

[11] S. S. Kim, H. Murayama, K. Kageyama, K. Uzawa, M. Kanai, Study on the curing process for carbon/epoxy composites to reduce thermal residual stress, Composites Part A: Applied Science and Manufacturing 43 (2012) 1197–1202. doi:10.1016/j.compositesa.2012.02.023.

[12] R. Prussak, D. Stefaniak, E. Kappel, C. Hühne, M. Sinapius, Smart cure cycles for fiber metal laminates using embedded fiber Bragg grating sensors, Composite Structures 213 (2019) 252–260. doi:10.1016/j.compstruct.2019.01.079.

[13] A. A. Johnston, An integrated model of the development of process-induced deformation in autoclave processing of composite structures, Dissertation, University of British Columbia, Vancouver, Kanada, 1997. doi:10.14288/1.0088805.

[14] Zapp Precision Metals GmbH, Rostfreier Federbandstahl 1.4310: Kennwerte für 1.4310, 2022. URL: https://www.zapp.com/fileadmin/_documents/Downloads/PS/informationsdatenblaetter/Federbandkatalog_PS.pdf.

[15] J. Wiedemann, J.-U. R. Schmidt, C. Hühne, Applicability of asymmetric specimens for residual stress evaluation in fiber metal laminates, Journal of Composites Science 6 (2022) 329. doi:10.3390/jcs6110329.

[16] J. Wiedemann, T. Barth, T. Roloff, T. Kluge, N. Rauter, C. Hühne, Influence of residual stresses on the dispersion behavior of guided ultrasonic waves in fiber metal laminates, in: Proceedings of the 14th International Workshop on Structural Health Monitoring, Destech Publications, Inc, 2023. doi:10.12783/shm2023/36729.

[17] B.-C. Chern, T. J. Moon, J. R. Howell, Measurement of the temperature and cure dependence of the thermal conductivity of epoxy resin, Experimental Heat Transfer 6 (1993) 157–174. doi:10.1080/08916159308946451.

[18] N. Slesinger, T. Shimizu, A. R. A. Arafath, A. Poursartip, Heat transfer coefficient distribution inside an autoclave, in: 17th International Conference On Composite Materials, 2009.

[19] T. Shimizu, J. C. Kotlik, A. R. A. Arafath, A. Poursartip, Evaluation of temperature profiles in thick composite parts during autoclave processing, in: A. C. Loos, M. W. Hyer, American Society for Composites (Eds.), ASC Series on Advances in Composite Materials: Manufacturing of Composites, Destech Publications Incorporated, 2013. URL: https://books.google.de/books?id=LjN7Vi5Mt4AC.

[20] J. Koord, Design methodology for highly loaded composite bolted joints with local metal hybridization at low temperature: DLR-Forschungsbericht - DLR-FB-2024-11, Dissertation, German Aerospace Center, Braunschweig, 2024. doi:10.57676/mzxc-3158.

[21] G. S. Springer, S. W. Tsai, Thermal conductivities of unidirectional materials, Journal of Composite Materials 1 (1967) 166–173. doi:10.1177/002199836700100206.